Pergamon

Acta mater. Vol. 46, No. 9, pp. 3077–3085, 1998

Printed in Great Britain
PII: S1359-6454(98)00007-X
1359-6454/98 $19.00 + 0.00

TRANSITION OF MECHANISMS CONTROLLING THE DISLOCATION MOTION IN CUBIC ZrO_2 BELOW 700°C

B. BAUFELD†, B. V. PETUKHOV‡, M. BARTSCH and U. MESSERSCHMIDT§
Max Planck Institute of Microstructure Physics, Weinberg 2, D-06120 Halle/Saale, Germany

(Received 18 August 1997; accepted in revised form 15 December 1997)

Abstract—For cubic ZrO_2 single crystals deformed in ⟨112⟩ direction, new experimental data are presented on the flow stress and its strain rate sensitivity as well as on the dislocation densities and the distances between glide obstacles along the dislocations. A model is proposed to describe the strong variation of the parameters of the plastic deformation below 1000 K. It assumes that the mechanisms controlling the dislocation motion change from the pinning by localized obstacles above a transition temperature, e.g. small precipitates or jogs, to the overcoming of the Peierls relief at lower temperatures. The model is in agreement with most of the experimental observations. © *1998 Acta Metallurgica Inc.*

1. INTRODUCTION

As it was shown earlier [1–3] (for a review, see [4]), cubic ZrO_2 single crystals exhibit a different plastic behavior in different temperature ranges. Above about 1500 K, the flow stress depends on the temperature and particularly on the strain rate [1, 2]. In an intermediate temperature range around about 1400 K, the deformation is of athermal character, and it becomes temperature-dependent again below about 1250 K [3, 4]. Accordingly, different mechanisms controlling the dislocation motion seem to cause this wide variation of the plastic properties of ZrO_2. At intermediate temperatures the plasticity is governed by the overcoming of long-range internal stresses between the dislocations, which undergo recovery processes at higher temperatures. Below 1250 K, the thermally activated overcoming of localized pinning centers is suggested to be the mechanism controlling the dislocation motion [3], and the glide velocity of dislocations can be described by an Arrhenius law

$$v = v_0 \exp\left\{-\frac{\Delta G(\tau^*)}{kT}\right\} = v_0 \exp\left\{-\frac{\Delta F(\tau^*) - V\tau^*}{kT}\right\}. \quad (1)$$

The parameters are: v_0 a preexponential factor, T the temperature, k the Boltzmann constant, $\Delta G(\tau^*)$ the Gibbs free energy and ΔF the Helmholtz free energy of activation, V the activation volume, and τ^* the effective shear stress, describing the temperature and strain rate sensitive part of the flow stress. The latter is the difference between the applied shear stress τ and the long-range internal stress τ_i

$$\tau^* = \tau - \tau_i. \quad (2)$$

The macroscopic plastic deformation rate $\dot{\varepsilon}$ can be described by the Orowan relation $\dot{\varepsilon} = \rho_m b v$, where ρ_m is the mobile dislocation density and b is the absolute value of the Burgers vector. Thus,

$$\dot{\varepsilon} = \dot{\varepsilon}_0 \exp\left\{-\frac{\Delta G(\tau^*)}{kT}\right\}. \quad (3)$$

Details of the dislocation glide mechanisms can be derived from the strain rate sensitivity, which is defined as

$$I = \Delta\sigma/\Delta\ln\dot{\varepsilon}. \quad (4)$$

σ is the applied (compression) stress, which is related to the shear stress τ via the orientation factor m_{SF} according to $\tau = m_{SF}\sigma$. The strong increase of the strain rate sensitivity by about two orders of magnitude in a relatively narrow temperature interval of about 300 K, which is obvious from the experiments quoted in [3] together with results from deformation tests performed between 823 K and 523 K under hydrostatic pressure to avoid brittle fracture [5, 6], and the corresponding change of the activation volume

$$V = kT/(m_{SF} I) \quad (5)$$

can hardly be explained solely within the framework of the model of the interaction between dislocations and local pinning centers. For thermally activated dislocation glide at a constant mobile

†Present address: Max Planck Institute of Metals Research, PML, P.O.B. 800665, Stuttgart, D-70506, Germany.
‡On leave from the Institute of Crystallography, Russian Academy of Sciences, Moscow.
§To whom all correspondence should be addressed.

dislocation density ρ_m, the activation volume is directly connected with the activation energy $\Delta G(\tau^*)$ to overcome the obstacles by $V = -\mathrm{d}\Delta G(\tau^*)/\mathrm{d}\tau^*$. Hence, the magnitude of the activation volume allows one to draw conclusions about the dislocation–obstacle interaction. The strongly increased strain rate sensitivity or the corresponding small activation volume at low temperatures therefore is evidence for a transition to another mechanism determining the dislocation mobility, which should be the lattice friction or Peierls mechanism (for reviews, see [7, 8]). Although the latter is suggested in [9] together with several other possible mechanisms controlling the dislocation mobility in ZrO_2 between 1381 K and 1708 K, in general, the role of the Peierls mechanism in the plasticity of ZrO_2 is not yet clear.

The present paper complements the data in [3, 5, 6] concerning deformation between 673 K and 873 K, and presents data on the obstacle distances and the total dislocation densities obtained by transmission electron microscopy. The dislocation densities allow one to estimate the internal stresses τ_i in equation (2). It is the aim of the paper to explain the strong variation of the deformation parameters of ZrO_2 around 800 K, to identify the mechanism of the low-temperature plasticity, and to quantitatively estimate its parameters on the basis of the theoretical considerations published in [10] on the transition from localized pinning of dislocations to the Peierls mechanism.

2. EXPERIMENTAL PROCEDURE AND RESULTS

This paper presents data on the flow stress σ and the strain rate sensitivity I of fully stabilized cubic ZrO_2 single crystals, which fill the gap between the results published in [3] and [5, 6], and originate from [11]. Similar to the previous paper [3], cubic ZrO_2 single crystals stabilized with 11 mol% Y_2O_3 were prepared for compression along the $[1\bar{1}2]$ direction. This orientation activates the primary $1/2[1\bar{1}0](001)$ slip system with a Schmid factor of $m_{SF} = 0.47$. The experiments were carried out in an Instron 8562 single-screw testing machine in air at temperatures between 673 K and 873 K. Figure 1 shows typical stress–strain curves for different temperatures together with previous curves below 1280 K from [3]. The strain rate sensitivity was obtained from strain rate cycling and stress relaxation experiments. After stress relaxation experiments and strain rate changes at higher temperatures yield drop phenomena occur, which vanish with decreasing temperature. The maximum stress difference was taken to determine the stress increments $\Delta\sigma$ in equation (4) for evaluating the strain rate cycling experiments. At low temperatures a prominent yield drop arises at the first loading. In Fig. 2, the flow stress $\sigma_{0.2}$ at a plastic strain of 0.2% is plotted vs temperature T. Besides, also flow

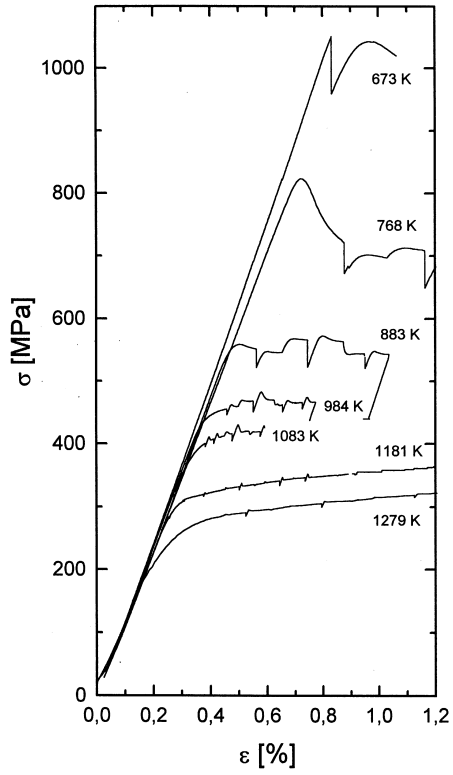

Fig. 1. Stress–strain curves of cubic ZrO_2–11 mol%Y_2O_3 at different temperatures, $\dot{\varepsilon} = 10^{-6}\ s^{-1}$, data from [3, 4, 11].

stress data are included which are measured under confining hydrostatic pressure [5, 6] as well as theoretical curves, which will be discussed below. The flow stress drastically increases with decreasing temperature, particularly below 800 K.

In the stress relaxation experiments, the total strain ε_t is kept constant ($\dot{\varepsilon}_t = 0$). Hence the plastic strain rate $\dot{\varepsilon}$ is proportional to the negative stress rate ($-\dot{\sigma}$) so that equation (4) reads

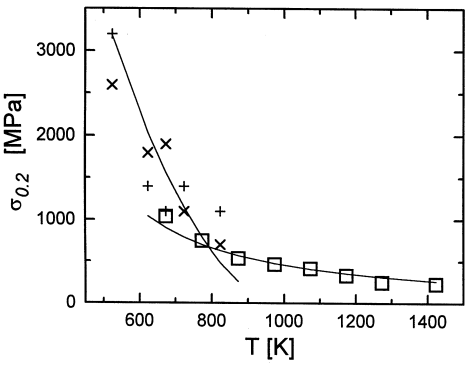

Fig. 2. Temperature dependence of the flow stress at a plastic strain of 0.2%. Symbols are experimental data at ambient atmosphere, $\dot{\varepsilon} = 10^{-6}\ s^{-1}$: □ 11 mol% Y_2O_3 [3, 4, 11]; and under confining hydrostatic pressure, $\dot{\varepsilon} = 2*10^{-4}\ s^{-1}$: + 12.6 mol%$Y_2O_3$, × 9.4 mol%$Y_2O_3$ [5, 6], The curves are the theoretical predictions for the Peierls mechanism at low temperatures and for localized obstacles at higher temperatures.

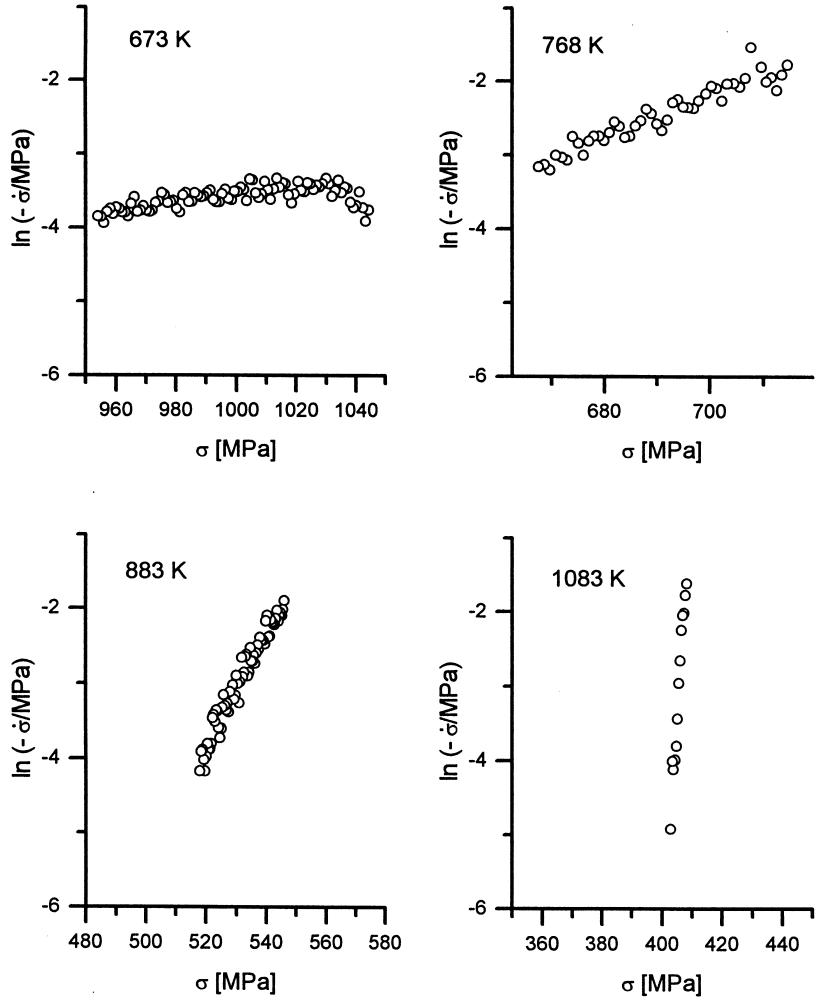

Fig. 3. Stress relaxation curves of ZrO_2 at different temperatures at a plastic strain of about 0.5% [4, 11].

$$I = \frac{\Delta\sigma}{\Delta \ln(-\dot{\sigma})}. \tag{6}$$

Thus, the inverse slope of plots of $\ln(-\dot{\sigma})$ vs σ equals the strain rate sensitivity. Figure 3 shows some typical stress relaxation curves for different temperatures. With decreasing temperature the slope of the curves drastically decreases. This corresponds to a strong increase of the strain rate sensitivity I as demonstrated in Fig. 4. Figure 4 also shows the data measured under hydrostatic pressure [5, 6] fitting those of the present study. The strain rate sensitivity seems to reach a constant value at the lowest temperatures. The small value of the activation volume V of less than $10b^3$ at low temperatures corresponding to the high strain rate sensitivity I is not easy to explain by the mechanism of localized obstacles, which is suggested for higher temperatures [3].

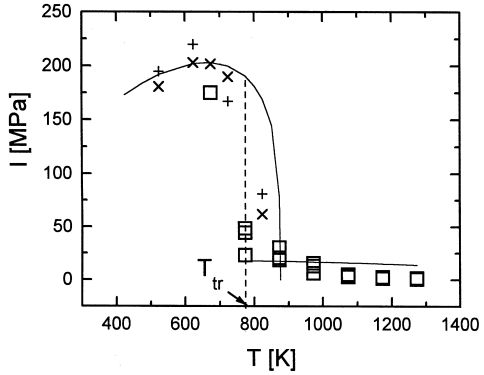

Fig. 4. Strain rate sensitivity of cubic ZrO_2–11 mol%Y_2O_3 in dependence on temperature [4–6, 11]. The curve is the theoretical dependence for the kink mechanism. Symbols as in Fig. 2.

Experimental activation energies Q_e were determined from temperature change experiments by

$$Q_e = -kT^2(\Delta\sigma/\Delta T)_{\dot{\varepsilon}}/I. \tag{7}$$

The Gibbs free energy of activation ΔG was calculated using the formalism described in [12]. In Fig. 5, it is plotted as a function of temperature. If

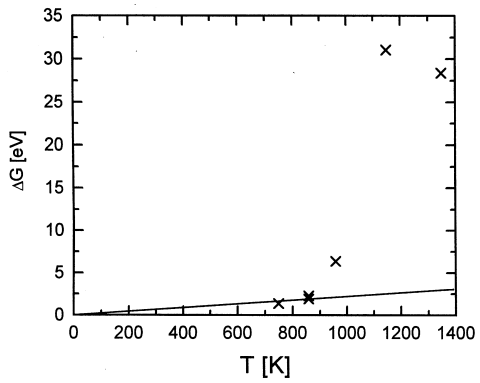

Fig. 5. Dependence of the Gibbs free energy of activation on the temperature.

the preexponential factor $\dot{\varepsilon}_0$ of the Arrhenius equation, equation (3), is constant this plot should be a straight line crossing the origin. This condition, including a reasonable slope, is only fulfilled up to 873 K. At higher temperatures, the activation energies take very high values owing to the low strain rate sensitivity I in equation (7). These very high values are not consistent with the model of thermally activated dislocation motion but hint at athermal processes in the range around 1250 K.

From the deformed specimens, samples were prepared for transmission electron microscopy. Two micrographs are shown in Fig. 6. At low temperatures, slip mainly occurs in narrow slip bands. Typically, the dislocations are of screw character [3, 11], partly appearing in dipole configurations, which indicates their mutual elastic interaction. Dislocation densities ρ were counted within the slip bands. As shown in Fig. 7, the dislocation density rises only very gradually with the temperature decreasing down to about 1000 K, but below this value it increases drastically. Internal stresses τ_i were calculated from the dislocation densities by means of a formula for Taylor hardening considering elastic anisotropy [4, 11]

$$\tau_i = \alpha K b F_m \rho^{1/2}/(2\pi). \tag{8}$$

Here, α is a numerical constant of about 8, K is the energy factor of screw dislocations (80.03 GPa at 873 K), which are typical of low temperature deformation, and $F_m = 0.3$ is a normalized maximum interaction force between parallel screw dislocations on {100} planes [4, 11]. Equation (8) and the dislocation densities in Fig. 7 are used to

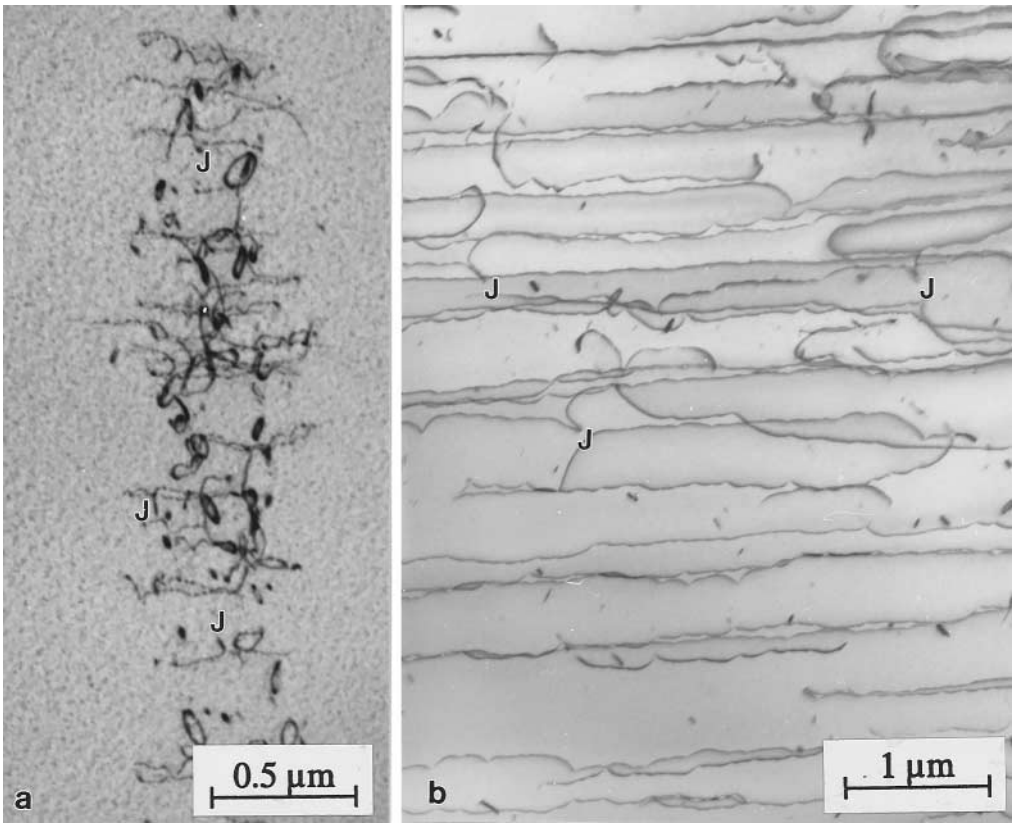

Fig. 6. Dislocation structures of specimens deformed in compression along [1$\bar{1}$2]. (a) 500°C. The specimen was cut parallel to a ($\bar{1}$11) plane. (b) 700°C. The specimen was cut parallel to the (001) slip plane. Some jogs are denoted by J. Please note the different scales in Figs 6(a) and (b).

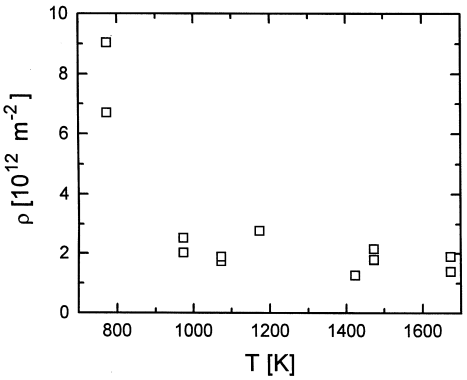

Fig. 7. Dependence of the dislocation density ρ inside slip bands on the temperature.

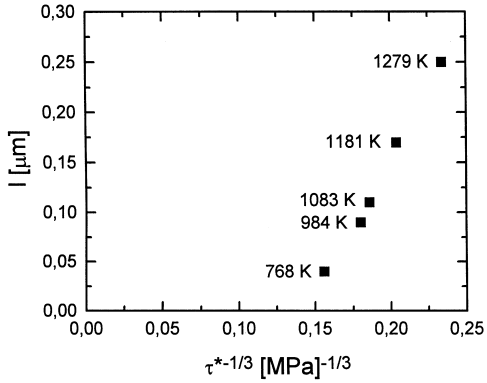

Fig. 8. Dependence of the obstacle distance l on the effective stress τ^* in a plot according to equation (21).

calculate the internal stresses, the result of which can be approximated by

$$\tau_i = 42\ \text{MPa} + 58.2\ \text{MPa}*\exp\{(787 - T\ [\text{K}])/135.6\}. \tag{9}$$

Below, this formula was used to calculate values of the effective stress τ^* from the applied stress τ by equation (2).

Characteristic of the dislocations at low temperatures is their curly shape as Fig. 6 demonstrates. It arises from the dislocations bowing out between obstacles, the nature of which is not yet fully understood. Some of them are clearly jogs but most of them seem to be localized obstacles as, e.g. small precipitates. In Fig. 8, the distance between the obstacles along the dislocations l is plotted vs $\tau^{*-1/3}$. The plot will be discussed in more detail below. Respective temperatures are indicated. The obstacle distance decreases with decreasing temperature.

In the following, a model will be described which explains the strong increase of the flow stress and, particularly, of its strain rate sensitivity with decreasing temperature. The results will be discussed in terms of the microstructural observations.

3. MODEL OF THE CHANGE OF THE MECHANISMS CONTROLLING THE DISLOCATION MOTION

At first, based on [10] the change of the rate-controlling mechanism of deformation is qualitatively discussed. It is suggested that the dislocations move under the simultaneous action of local pinning centers and the Peierls mechanism. Both the shape of the dislocations and the value of the activation volume indicate that above 973 K the dislocation motion is governed by the overcoming of local pinning centers with a characteristic waiting time t_l at the obstacles. In accordance with equation (1), one obtains

$$\begin{aligned} 1/t_l &= \nu_0 \exp\left\{-\frac{\Delta G_l(\tau^*)}{kT}\right\} \\ &= \nu_0 \exp\left\{-\frac{\Delta F_l(\tau^*) - V\tau^*}{kT}\right\} \\ &= \nu_0 \exp\left\{-\frac{\Delta F_l(\tau^*) - df}{kT}\right\}. \end{aligned} \tag{10}$$

ν_0 is an attempt frequency, d is the so-called activation distance, and f is the force acting on the obstacles. The other symbols are the same as in equation (1). The flight time t_p of the dislocation segments between the pinning centers is considered negligible: $t_p \ll t_l$. Although this motion may require thermal activation to overcome the Peierls barriers, at sufficiently high temperatures this process proceeds at a high rate and does not retard the dislocation motion remarkably. The dislocation segments bow out, assuming their equilibrium shapes in a time rather short compared to that of overcoming the pinning centers. At lower temperatures, however, the relation between t_l and t_p may be reversed. This is illustrated in Fig. 9, where the dependencies of the respective activation energies of

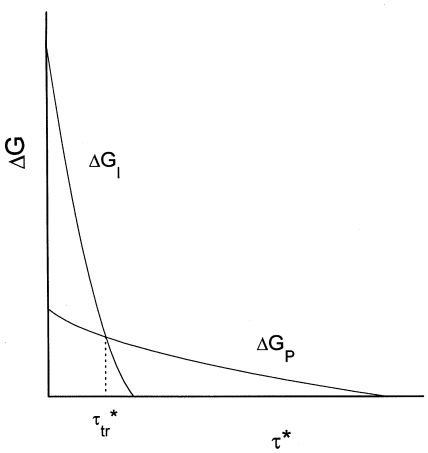

Fig. 9. Schematic stress dependencies of energy profiles for local pinning $\Delta G_l(\tau^*)$ and the Peierls mechanism $\Delta G_P(\tau^*)$.

both processes, $\Delta G_l(\tau^*)$ and $G_p(\tau^*)$, on stress are schematically shown.

At high temperatures corresponding to low stresses, ΔG is large with the localized obstacles attributing the main resistance to dislocation motion. Here, the force f which the dislocations exert on the obstacles under the action of the effective stress τ^* is proportional to the average distance l between the pinning centers, i.e. $f = \tau^* bl$, corresponding to a relatively large activation volume $V = dbl$. Accordingly, $\Delta G_l(\tau^*)$ strongly decreases with increasing stress or decreasing temperature. At a transition stress τ_{tr}^*, it becomes equal to $\Delta G_p(\tau^*)$, which is the activation energy of the kink pair generation, i.e. of the Peierls mechanism. At low temperatures and high stresses, when $\tau^* > \tau_{tr}^*$, most of the dislocation retardation is due to this slow motion of the dislocation segments between the pinning points. Then, the forces acting on the obstacles that adjoin the slowly moving dislocation segment are gradually increasing. Near the transition temperature, corresponding to τ^*_{tr}, the deformation behavior may drastically change. Particularly the activation volume may drop from large values typical of overcoming local pinning centers to small values of a few b^3 typical of the Peierls mechanism. The strain rate sensitivity will change correspondingly.

After the above qualitative picture, a more detailed description will follow, taking into account the mutual influence of the two mechanisms on each other. If the Peierls mechanism is neglected there will be only a single equilibrium configuration of a dislocation segment bowing out under stress. In the more general case, owing to the periodic Peierls relief, many locally stable (or metastable) configurations of the dislocation segment appear, which may be characterized by their bowing height h at the center of the segments as shown in Fig. 10. The bowing height is given by $h \cong na + y_n$ with $n = 1, 2, 3, \ldots, n_e$. a is the period of the Peierls relief $U_P(y)$ and y_n is the shift of the dislocation from the bottom of the Peierls potential to reach the force equilibrium according to $dU_P(y_n)/dy = \tau^* b$. $h_e = n_e a \cong l^2 \tau^* b/8\kappa$ describes the final equilibrium bowing, which corresponds to the energetically most favorable configuration of the dislocation segment, i.e. to the equilibrium configuration without the Peierls relief. κ is the line tension. In the line tension approximation, the curved segment of the dislocation near the local obstacle can be described by the equilibrium equation for a relatively small bowing:

$$\kappa y''(x) - \frac{dU_P(y)}{dy} + \tau^* b = 0. \tag{11}$$

Here, $y(x)$ is the dislocation displacement at the point x, and $y''(x) = d^2y/dx^2$. The first integral of equation (11) is

$$\frac{\kappa}{2} y'^2 - U_P(y) + \tau^* b y = \text{const.} \tag{12}$$

The integration constant is determined from the bowing height h of the dislocation segment between the pinning points, which corresponds to the condition $y'(h) = 0$. Thus, const $= -U_P(h) + \tau^* bh$. Equation (12) yields the slope $y' = dy/dx$ of the dislocation segments near the pinning points, which determines the contact force of equation (10)

$$f = 2\kappa \frac{dy}{dx} \sqrt{8\kappa [U_P(y) - U_P(h) + \tau^* b(h - y)]} \tag{13}$$

which the dislocation exerts on the pinning centers. This formula shows the influence of the lattice relief on the force acting on the obstacles: both mechanisms are not simply additive. For $U_P(y) = 0$, h will immediately assume its equilibrium value h_e, yielding the well-known result $f = \tau^* bl$ for the absence of the Peierls relief. In general, however, the magnitude of f depends on the position of the dislocation in the Peierls relief. When the dislocation first contacts the obstacles, this force f is small. Afterwards, it increases step by step as the dislocation proceeds from one Peierls valley to the next one.

The integration of equation (12) determines the stable positions possible of the dislocation segment between the pinning centers

$$x = \pm \int_h^y \frac{dy_1}{\sqrt{(2/\kappa)[U_P(y_1) - U_P(h) + \tau^* b(h - y_1)]}}. \tag{14}$$

Examples of such configurations with a straightened top are shown in Fig. 10 for several values of h. A harmonic Peierls potential

$$U_P(y) = \frac{\tau_P ab}{2\pi} \left(1 - \cos\left(2\pi \frac{y}{a}\right)\right) \tag{15}$$

was used with the parameters $\tau^* = 0.1\tau_P$ and $l = 7(\kappa a/\tau_P b)^{1/2}$. τ_P is the Peierls stress.

The dislocation segment has a finite lifetime t_p in each locally stable position corresponding to a certain value of h. While staying in such a position, a competition takes place between the two thermally activated processes of shifting the dislocation segment to the next Peierls valley by the nucleation

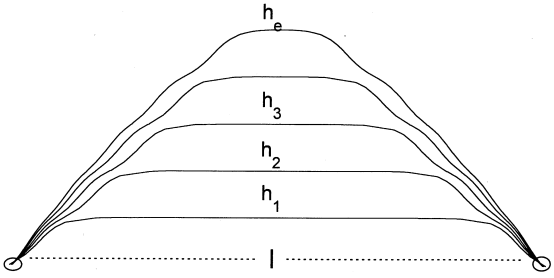

Fig. 10. Stable or metastable dislocation configurations at the combined action of localized obstacles and the Peierls mechanism.

of a kink pair, or of overcoming one of the adjacent obstacles, which is connected with the waiting time t_l. According to equations (10) and (13), t_l becomes shorter and shorter as the dislocation proceeds and h increases. As soon as t_l becomes approximately equal to t_p, one of the neighboring obstacles is overcome before the equilibrium value h_e of the bowing-out is reached. Then, the dislocation mobility is determined by the kinetics of the bowing, which depends on the rate of overcoming the Peierls barriers due to the formation of kink pairs with a formation energy $\Delta G_p(\tau^*)$ (see, e.g. Refs [8, 9]). The reciprocal value of the waiting time t_p of a dislocation segment to overcome a position of a certain value of h is proportional to the Arrhenius factor $\exp(-\Delta G_p(\tau^*)/kT)$ and to its length l owing to the so-called "length effect" [8]. This effect follows from the possibility that a kink pair may form at any site along the dislocation segment. As l enters only the preexponential factor of the equation of the dislocation mobility and does not change the activation energy, this effect is of minor importance. Therefore, if the difference between the preexponential factors in the Arrhenius equations of $1/t_l$ and $1/t_p$ is neglected, the transition between both mechanisms takes place at $\Delta G_l \cong \Delta G_p$, or at $\tau^* = \tau^*_{tr}$ as discussed before in connection with Fig. 9. At $\tau^* > \tau^*_{tr}$, the activation volume takes the usual values of the Peierls mechanism, which are much smaller than those for overcoming the localized obstacles. According to equation (6), this drop of the activation volume at $\tau^* = \tau^*_{tr}$ is accompanied by a strong increase of the strain rate sensitivity I.

At $\tau^* > \tau^*_{tr}$, the plastic strain rate $\dot{\varepsilon}$ is determined by an Arrhenius law similar to equation (3), with the kink pair nucleation energy $\Delta G_p(\tau^*)$:

$$\dot{\varepsilon} = \dot{\varepsilon}_0 \exp(-\Delta G_p(\tau^*)/kT). \qquad (16)$$

The preexponential factor $\dot{\varepsilon}_0$ is considered constant, and, as mentioned before, its possible change at the transition is not taken into account. The stress dependence of the kink pair formation energy can be calculated for any type of the Peierls relief $U_P(y)$ using a formula suggested in [13]

$$\Delta G_p(\tau^*) = \int \sqrt{2\kappa[U_P(y) - \tau^* b y]}\, dy. \qquad (17)$$

4. APPLICATION OF THE MODEL TO THE PLASTICITY OF CUBIC ZrO_2

In the following, an attempt will be made to interpret semiquantitatively the experimental results presently available on the low-temperature plasticity of cubic ZrO_2, using the model outlined in Section 3. In Section 2, these experimental results were described comprising the macroscopic data on the flow stress and its strain rate sensitivity in Figs 2 and 4, and the information on the internal stress of equation (9) based on the dislocation densities presented in Fig. 7. To this end, equation (17) will be approximated by

$$\Delta G_P(\tau^*) = 2\Delta G_k(1 - (\tau^*/\tau_P)^{4/5})^{5/4}, \qquad (18)$$

where ΔG_k is the kink energy. Equation (18) is a good approximation of the general equation (17) for the harmonic Peierls potential of equation (15), providing a convenient analytical expression of the stress dependence of the activation energy.

The transition temperature between the dominance of localized obstacles and the Peierls mechanism was estimated to be $T_{tr} = 773$ K. Considering equation (2) for adding the effective stress τ^* and the internal stress τ_i and equation (9) for the dependence of τ_i on temperature, the low-temperature flow stress data are best fitted by equations (16) and (18) using the parameters $\tau_p = 4500$ MPa, $2\Delta G_k = \Delta G_p(\tau^* = 0) = 1.8$ eV, and $T^* = 2\Delta G_k/(k \ln(\dot{\varepsilon}_0/\dot{\varepsilon})) = 875$ K. Like in [3], the high-temperature data are fitted by equation (3) and an empirical potential proposed in [14]

$$\Delta G(\tau^*) = \Delta G_0 \left(1 - \left(\frac{\tau^*}{\tau_0}\right)^{1/2}\right)^{3/2}, \qquad (19)$$

with parameters close to those estimated previously [3]: $\Delta G_0 = 4.2$ eV and $\tau_0 = 1760$ MPa. In Fig. 2, both expressions are plotted in full lines.

The same parameters are used to calculate the strain rate sensitivity I. Figure 4 shows the curves together with the experimental data available including the transition temperature indicated by a dashed line. According to the theory of the Peierls mechanism, the calculated curve ends at $T^* = 875$ K. In spite of their scattering, the experimental data in Fig. 4 clearly show that I strongly increases with the temperature decreasing below 875 K. The temperature of the maximum gradient coincides with the transition temperature $T_{tr} = 773$ K. The curve of the Peierls mechanism also well describes constant, or even decreasing, values of I at the lowest temperatures. Above the transition temperature, at increasing temperature the experimental values of I decrease more strongly than the theoretical curve.

5. DISCUSSION

The model proposed of dislocations moving under the simultaneous action of local pinning centers and an extended Peierls relief explains the drastic changes of the flow stress and, particularly, of the strain rate sensitivity of cubic ZrO_2 in a narrow temperature range. The drastic drop of the activation volume to values in the order of a few b^3 and the strong temperature dependence of the flow stress suggest that at low temperatures dislocation glide is controlled by lattice friction. The Peierls mechanism is not directly proven by microscopic

results, i.e. there are no straight dislocation segments arranged in preferred crystallographic orientations. Some preference of the ⟨100⟩ orientations can already be explained by the anisotropic line tension on the {001} slip planes [4, 11]. However, the fact that bowed-out dislocation configurations do not significantly relax after unloading the samples indirectly hints at a strong friction, which most probably is the Peierls mechanism. The operation of the Peierls mechanism at low temperatures was already concluded in [15]. In this work, the Peierls stress for the {001} plane was estimated to amount to about 4 GPa ($5 \times 10^{-2}\,\mu$) from an extrapolation of the flow stress data then available in a plot of $\ln\sigma$ vs T or to 7.2 GPa from a simplified Peierls model.

The parameters estimated of the Peierls mechanism, i.e. the Peierls stress τ_P and the kink energy ΔG_k, appear as independent parameters in equation (18). According to the line tension theory of the Peierls mechanism (e.g. [7]), however, they are linked by

$$\Delta G_k = (Ca/\pi)(2U_{P,max}\kappa)^{1/2}, \tag{20}$$

with $C = 2$ and $U_{P,max} = \tau_P ab/\pi$ (see equation (15)). Taking $\kappa = (Kb^2/4\pi)\ln(l/5b)$ for the line tension of bowed-out segments of length l ($\cong 0.1\,\mu$m), the numerical values of ΔG_k and τ_P are not consistent. The present value of τ_P then implies that ΔG_k would be twice as high as it was estimated above. In a more recent work [16], the line tension model of the Peierls mechanism is compared with a model of discrete double-kinks of trapezoidal shape using different forms of the Peierls potential. Figure 2 of this paper confirms the above functional relation between ΔG_k and τ_P. However, the constant C may vary by a factor of about two, depending on a cut-off parameter. Using the expression of isotropic elasticity for the line tension, this wide variation of C is necessary to explain the low temperature flow stress data of different b.c.c. metals. Thus, the inconsistency of the evaluated data in terms of the simple line tension model of the Peierls mechanism is certainly a limitation of the theory but does not contradict the conclusion that the Peierls mechanism controls the flow stress of cubic zirconia at low temperatures.

The accuracy of both parameters, τ_P and ΔG_k, however, is quite different. Determining the Peierls stress requires a long extrapolation to zero temperature, the result of which may be influenced, e.g. by the particular choice of the Peierls potential. Thus, the obtained Peierls stress of $\tau_P = 4500$ MPa should be considered a rough estimate. It is about 6% of K, which is a high but not unreasonably high value. Similarly, the Peierls potential amounts to about 3% of the line tension. On the other hand, the kink energy is derived from the transition temperature T_{tr}, which follows from a short interpolation of the experimental data in the transition range. That makes the estimation of the kink energy $\Delta G_k = 0.9$ eV quite reliable. Using this value, one may conclude that the kink density along the dislocations is sufficiently high above about 900 K so that the kink generation does not control the dislocation mobility at higher temperatures. This clearly shows that the Peierls mechanism with its parameters determined at low temperatures cannot control the dislocation mobility in the temperature range between 1381 K and 1708 K, as it was proposed in [9].

The present approach does not consider the combination of two mechanisms of impeding the dislocation motion a simple addition of the two stress contributions corresponding to both mechanisms separately. Such an oversimplified approach does not take into account the plastic behavior near the transition from one mechanism controlling the dislocation mobility to the other one. In Section 4, the numerical data of the model are estimated by fitting the experimental data outside the transition temperature range. A more exact evaluation of the transition range itself has still to be done on the basis of equation (13). Nevertheless, the strong variation of the strain rate sensitivity in the transition range should correspond to the discussed change of the mechanisms controlling the dislocation motion. Most probably, this change is the reason for the low-temperature brittleness of ZrO_2 owing to the strong increase of the flow stress at $T < T_{tr}$.

While the interpretation of the macroscopic deformation data at temperatures below T_{tr} by the Peierls mechanism is quite straightforward, problems arise for the range between T_{tr} and about 1100 K. There is strong microscopic evidence that localized obstacles determine the bowed-out dislocation configurations above T_{tr} (e.g. Figure 6). However, the nature of these obstacles is not clear yet. Most of them are supposed to be small precipitates, possibly containing nitrogen [17]. Although they certainly control also the dislocation mobility, a single set of parameters of equation (19) was not found to equally well fit the flow stress data of Fig. 2 and the strain rate sensitivity data of Fig. 4. Besides, if the pre-exponential factor of the Arrhenius equation (3) is considered constant, as presently done, the plot of the Gibbs free energy of activation ΔG vs temperature T should be a straight line through the origin. The slope of the line characterizes the pre-exponential factor. The line drawn in Fig. 5 corresponds already to a very high pre-exponential factor. The values of ΔG above about 870 K, however, are unreasonably high in terms of the models of thermally activated dislocation motion. They do not result from a high temperature sensitivity of the flow stress but from a very low strain rate sensitivity I. This is characteristic of athermal processes that dominate in the temperature range around 1250 K [4, 11]. Another

problem is the dependence of the obstacle distance l on the effective stress τ^* as shown in Fig. 8. For an array of a single type of localized obstacles, i.e. of obstacles of unique strength, this dependence should be represented by the so-called Friedel relation [18, 19] (for a review, see [14])

$$l = \alpha l_{sq}^{2/3}\{2\kappa/(\tau^* b)\}^{1/3}. \quad (21)$$

Here, α is a numerical factor near unity and l_{sq} is the so-called square lattice distance. l_{sq}^2 is the average area of the slip plane per obstacle. Figure 8 is a plot of l vs $\tau^{*-1/3}$. The experimental data do not form a straight line through the origin as it was expected from equation (21). This discrepancy certainly has several reasons. Some of the pinning agents in Fig. 6 can clearly be identified as jogs. They are labelled by J. It is possible that the density of jogs along the dislocations increases with decreasing temperature. Besides, the localized obstacles are not necessarily of unique strength so that the spectrum of active obstacles may change with temperature.

In spite of these discrepancies regarding the details of the mechanism of localized obstacles, the main result of this work, i.e. the transition from an extrinsic mechanism controlling the dislocation motion at temperatures above about 800 K to the intrinsic lattice friction below that temperature, is quite obvious.

6. CONCLUSIONS

— The flow stress of cubic zirconia for glide on {001} planes strongly increases below about 800 K.

— The strain rate sensitivity of the flow stress increases by more than one order of magnitude in a small temperature interval around 800 K and is constant, or even slightly decreases, below about 600 K.

— A model is presented to explain these drastic changes by the transition from localized obstacles above 800 K to the Peierls mechanism at lower temperatures, controlling the dislocation mobility.

— The numerical evaluation considers also long-range internal stresses derived from the dislocation densities.

— Though transmission electron microscopy proves that localized obstacles determine the shape of dislocations, details of this mechanism are at variance.

Acknowledgements—One of the authors (B. V. P.) acknowledges the kind hospitality of the Max Planck Institute of Microstructure Physics during the course of this work. Financial support of the Deutsche Forschungsgemeinschaft is gratefully acknowledged.

REFERENCES

1. Cheong, D.-S., Dominguez-Rodriguez, A. and Heuer, A. H., *Philos. Mag. A*, 1991, **63**, 377.
2. Messerschmidt, U., Baufeld, B., McClellan, K. J. and Heuer, A. H., *Acta metall. mater.*, 1995, **43**, 1917.
3. Baufeld, B., Bartsch, M., Messerschmidt, U. and Baither, D., *Acta metall. mater.*, 1995, **43**, 1925.
4. Messerschmidt, U., Baufeld, B. and Baither, D., in *Zirconia Engineering Ceramics: Old Challenges — New Ideas*, ed. E. Kisi. Trans. Tech. Publ., in press.
5. Teracher, P., Garem, H. and Rabier, J., in *Strength of Metals and Alloys*, ed. D. G. Brandon, R. Chaim and A. Rosen. Freund Publs. London, 1991, p. 217.
6. Teracher, P., Ph. D. Thesis, Poitiers, 1990.
7. Hirth, J. P. and Lothe, J., *Theory of Dislocations*. Wiley, New York, 1982, p. 531.
8. Seeger, A., in *Dislocations*, ed. P. Veyssiere, L. Kubin and J. Castaing. CNRS, Paris, 1984.
9. Farber, B. Ya., Chiarelli, A. S. and Heuer, A. H., *Philos. Mag. A*, 1995, **72**, 59.
10. Petukhov, B. V., *Crystallogr. Rep.*, 1996, **41**, 197.
11. Baufeld, B., Doctoral Thesis, Halle (Saale), 1996.
12. Schoeck, G., *Phys. status solidi*, 1965, **8**, 499.
13. Celli, V., Kabler, M., Ninomiya, T. and Thomson, R., *Phys. Rev.*, 1963, **131**, 58.
14. Kocks, U. F., Argon, A. S. and Ashby, M. F., in *Thermodynamics and Kinetics of Slip*, Vol. 19, ed. B. Chalmers, J. W. Christian and T. B. Massalski, Prog. in Mater. Sci. Pergamon Press, Oxford, 1975.
15. Dominguez-Rodriguez, A., Heuer, A. H. and Castaing, J., *Radiat. Eff. Defects Solids*, 1991, **119-121**, 759.
16. Suzuki, T., Koizumi, H. and Kirchner, H. O. K., *Acta metall. mater.*, 1995, **43**, 2187.
17. Gomez-Garcia, D., Martinez-Fernandez, J., Dominguez-Rodriguez, A. and Westmacott, K., *J. Am. Ceram. Soc.*, 1996, **79**, 487.
18. Morris, J. W. and Klahn, D. H., *J. Appl. Phys.*, 1974, **45**, 2027.
19. Labusch, R., *J. Appl. Phys.*, 1977, **48,** 4550.